Heavy Quark Production in the ACOT Scheme at NNLO and N³LO

T. Stavreva,[1, *] F. I. Olness,[2, †] I. Schienbein,[1, ‡] T. Ježo,[1, §] A. Kusina,[2, ¶] K. Kovařík,[3, **] and J. Y. Yu[2, 1, ††]

[1]*Laboratoire de Physique Subatomique et de Cosmologie, Université Joseph Fourier/CNRS-IN2P3/INPG,*
53 Avenue des Martyrs, 38026 Grenoble, France
[2]*Southern Methodist University, Dallas, TX 75275, USA*
[3]*Institute for Theoretical Physics, Karlsruhe Institute of Technology, Karlsruhe, D-76128, Germany*

We analyze the properties of the ACOT scheme for heavy quark production and make use of the $\overline{MS}$ massless results at NNLO and N³LO for the structure functions F_2 and F_L in neutral current deep-inelastic scattering to estimate the higher order corrections. For this purpose we decouple the heavy quark mass entering the phase space from the one entering the dynamics of the short distance cross section. We show numerically that the phase space mass is generally more important. Therefore, the dominant heavy quark mass effects at higher orders can be taken into account using the massless Wilson coefficients together with an appropriate slow-rescaling prescription implementing the phase space constraints. Combining the exact ACOT scheme at NLO with these expressions should provide a good approximation to the missing full calculation in the ACOT scheme at NNLO and N³LO.

CONTENTS

---

[*] stavreva@lpsc.in2p3.fr

[†] olness@smu.edu

[‡] schien@lpsc.in2p3.fr

[§] jezo@lpsc.in2p3.fr

[¶] akusina@smu.edu

[**] kovarik@particle.uni-karlsruhe.de

[††] yu@physics.smu.edu

I. INTRODUCTION

A. Motivation

The production of heavy quarks in high energy processes has become an increasingly important subject of study both theoretically and experimentally. The theory of heavy quark production in perturbative Quantum Chromodynamics (pQCD) is more challenging than that of light parton (jet) production because of the new physics issues brought about by the additional heavy quark mass scale. The correct theory must properly take into account the changing role of the heavy quark over the full kinematic range of the relevant process from the threshold region (where the quark behaves like a typical "heavy particle") to the asymptotic region (where the same quark behaves effectively like a parton, similar to the well known light quarks $\{u, d, s\}$).

With the ever-increasing precision of experimental data and the progression of theoretical calculations and parton distribution function (PDF) evolution to next-to-next-to-leading order (NNLO) of QCD there is a clear need to formulate and also implement the heavy quark schemes at this order and beyond. The most important case is arguably the heavy quark treatment in inclusive deep-inelastic scattering (DIS) since the very precise HERA data for DIS structure functions and cross sections form the backbone of any modern global analysis of PDFs. Here, the heavy quarks contribute up to 30% or 40% to the structure functions at small momentum fractions x. Extending the heavy quark schemes to higher orders is therefore necessary for extracting precise PDFs and hence for precise predictions of observables at the LHC. However, we would like to also stress the theoretical importance of having a general pQCD framework including heavy quarks which is valid to all orders in perturbation theory over a wide range of hard energy scales and which is also applicable to other observables than inclusive DIS in a straightforward manner.

An example, where higher order corrections are particularly important is the structure function F_L in DIS. The leading order ($\mathcal{O}(\alpha_S^0)$) contribution to this structure function vanishes for massless quarks due to helicity conservation (Callan-Gross relation). This has several consequences:

- F_L is useful for constraining the gluon PDF via the dominant subprocess $\gamma^* g \to q\bar{q}$.

- The heavy quark mass effects of order $\mathcal{O}(\frac{m^2}{Q^2})$ are relatively more pronounced.[1]

---

[1] Similar considerations also hold for target mass corrections (TMC) and higher twist terms. We focus here mainly on the kinematic region $x < 0.1$ where TMC are small [1]. An inclusion of higher twist terms is beyond the scope of this study.
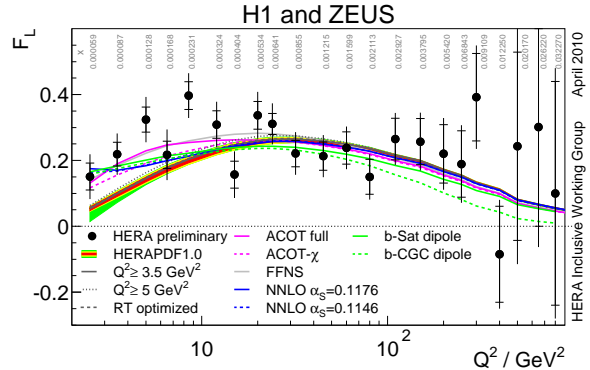

Figure 1: F_L vs. Q from combined HERA-I inclusive deep inelastic cross sections measured by the H1 and ZEUS collaborations. Figure taken from Ref. [2].

- Since the first non-vanishing contribution to F_L is next-to-leading order (up to mass effects), the NNLO and N³LO corrections are more important than for F_2.

In Fig. 1 we show a comparison of different theoretical calculations of F_L with preliminary HERA data [2]. As can be seen, in particular at small Q^2 (i.e. small x), there are considerable differences between the predictions.[2]

The purpose of this paper is to calculate the leading twist neutral current DIS structure functions F_2 and F_L in the ACOT factorization scheme up to order $\mathcal{O}(\alpha_S^3)$ (N³LO) and to estimate the error due to approximating the heavy quark mass terms $\mathcal{O}(\alpha_S^2 \times \frac{m^2}{Q^2})$ and $\mathcal{O}(\alpha_S^3 \times \frac{m^2}{Q^2})$ in the higher order corrections. The results of this study form the basis for using the ACOT scheme in NNLO global analyses and for future comparisons with precision data for DIS structure functions.

B. Outline of Paper

The rest of this paper is organized as follows. In Sec. II we review theoretical approaches to include heavy flavors in QCD calculations. Particular emphasis is put on the ACOT scheme which is the minimal extension of the $\overline{MS}$ scheme in the sense that the observables in the ACOT scheme reduce to the ones in the $\overline{MS}$ scheme in the limit $m \to 0$ without any finite renormalizations. In this discussion we explicitly distinguish between the heavy quark/heavy meson mass entering the final state phase space which we will call "phase space mass" and the heavy quark mass entering the dynamics of the short

---

[2] An updated analysis of the H1 measurements extending down to even lower Q^2 values has been published in Ref. [3], and a combined analysis with ZEUS is in progress.
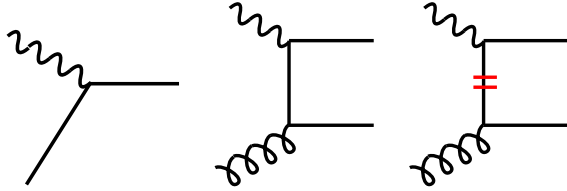
Figure 2: Characteristic Feynman graphs which contribute to DIS heavy quark production in the ACOT scheme: a) the LO $\mathcal{O}(\alpha_S^0)$ quark-boson scattering $QV \to Q$, b) the NLO $\mathcal{O}(\alpha_S^1)$ gluon-boson scattering $gV \to Q\bar{Q}$, and c) the corresponding subtraction term (SUB) $(g \to Q\bar{Q}) \otimes (Q \to gQ)$.

distance cross section denoted "dynamic mass." We show numerically using the exact ACOT scheme at $\mathcal{O}(\alpha_S)$ (NLO) that the effects of the phase space mass are more important than the ones due to the dynamic mass. We use this observation to construct in Sec. III the NC DIS structure functions in the ACOT scheme up to $\mathcal{O}(\alpha_S^3)$. The corresponding numerical results are presented in Sec. IV. Finally, in Sec. V we summarize the main results.

II. REVIEW OF THEORETICAL METHODS

We review theoretical methods which have been advanced to improve existing QCD calculations of heavy quark production, and the impact on recent experimental results.

A. ACOT Scheme

The ACOT renormalization scheme [4] provides a mechanism to incorporate the heavy quark mass into the theoretical calculation of heavy quark production both kinematically and dynamically. In 1998 Collins [5] extended the factorization theorem to address the case of heavy quarks; this work provided the theoretical foundation that allows us to reliably compute heavy quark processes throughout the full kinematic realm.

Figure 2 displays characteristic Feynman graphs for the first two orders of DIS heavy quark production. If we consider the DIS production of heavy quarks at $\mathcal{O}(\alpha_S^1)$ this involves the LO $QV \to Q$ process and the NLO $gV \to Q\bar{Q}$ process.[3]

The key ingredient provided by the ACOT scheme is the subtraction term (SUB) which removes the "double

counting" arising from the regions of phase space where the LO and NLO contributions overlap. Specifically, at NLO order, we can express the total result as a sum of

$$\sigma_{TOT} = \sigma_{LO} + \{\sigma_{NLO} - \sigma_{SUB}\} \qquad (1)$$

where the subtraction term for the gluon-initiated processes is

$$\sigma_{SUB} = f_g \otimes \tilde{P}_{g \to Q} \otimes \sigma_{QV \to Q}. \qquad (2)$$

σ_{SUB} represents a gluon emitted from a proton (f_g) which undergoes a collinear splitting to a heavy quark $(\tilde{P}_{g \to Q})$ convoluted with the LO quark-boson scattering $\sigma_{QV \to Q}$. Here, $\tilde{P}_{g \to Q}(x, \mu) = \frac{\alpha_s}{2\pi} \ln(\mu^2/m^2) P_{g \to Q}(x)$ where $P_{g \to Q}(x)$ is the usual $\overline{MS}$ splitting kernel, m is the quark mass and μ is the renormalization scale[4] which we typically choose to be $\mu = Q$.

An important feature of the ACOT scheme is that it reduces to the appropriate limit both as $m \to 0$ and $m \to \infty$ as we illustrate below.

1. Fixed-Flavor-Number-Scheme (FFNS) Limit

Specifically, in the limit where the quark Q is relatively heavy compared to the characteristic energy scale $(\mu \lesssim m)$, we find $\sigma_{LO} \sim \sigma_{SUB}$ such that $\sigma_{TOT} \sim \sigma_{NLO}$. In this limit, the ACOT result naturally reduces to the Fixed-Flavor-Number-Scheme (FFNS) result. In the FFNS, the heavy quark is treated as being extrinsic to the hadron, and there is no corresponding heavy quark PDF $(f_Q \sim 0)$; thus $\sigma_{LO} \sim 0$. We also have $\sigma_{SUB} \sim 0$ because this is proportional to $\ln(\mu^2/m^2)$. Thus, when the quark Q is heavy relative to the characteristic energy scale μ, the ACOT result reduces to $\sigma_{TOT} \sim \sigma_{NLO}$.

2. Zero-Mass Variable-Flavor-Number-Scheme (ZM-VFNS) Limit

Conversely, in the limit where the quark Q is relatively light compared to the characteristic energy scale $(\mu \gtrsim m)$, we find that σ_{LO} yields the dominant part of the result, and the "formal" NLO $\mathcal{O}(\alpha_S)$ contribution $\{\sigma_{NLO} - \sigma_{SUB}\}$ is an $\mathcal{O}(\alpha_S)$ correction.

In the limit $m/\mu \to 0$, the ACOT result will reduce to the $\overline{MS}$ Zero-Mass Variable-Flavor-Number-Scheme (ZM-VFNS) limit exactly without any finite renormalizations. In this limit, the quark mass m no longer plays any dynamical role and purely serves as a regulator. The σ_{NLO} term diverges due to the internal exchange of the quark Q, and this singularity will be canceled by σ_{SUB}.

---

[3] At NLO, there are corresponding quark-initiated terms; for simplicity we do not display them here, but they are fully contained in our calculations [6].

[4] In this subsection we will distinguish μ and Q; in the following, we will set $\mu = Q$ and display the results as a function of Q.
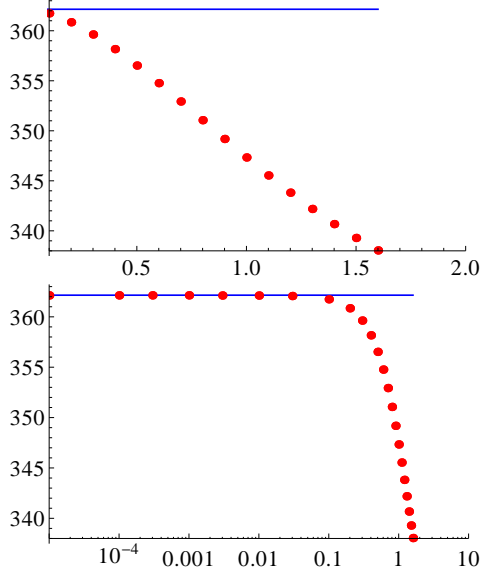
Figure 3: Comparison of $F_2^c(x, Q)$ (scaled by 10^4) vs. the quark mass m in GeV for fixed $x = 0.1$ and $Q = 10$ GeV. The red dots are the full ACOT result, and the blue line is the massless $\overline{MS}$ result. The logarithmic plot demonstrates this result holds precisely in the $m \to 0$ limit.

3. ACOT as a minimal extension of $\overline{MS}$

We illustrate the versatile role of the quark mass in Fig. 3-a where we display the $\overline{MS}$ ZM-VFNS and the ACOT result as a function of the quark mass m.

We observe that when m is within a decade or two of μ that the quark mass plays a dynamic role; however, for $m \ll \mu$, the quark mass purely serves as a regulator and the specific value is not important. Operationally, it means we can obtain the $\overline{MS}$ ZM-VFNS result either by i) computing the terms using dimensional regularization and setting the regulator to zero, or ii) by computing the terms using the quark mass as the regulator and then setting this to zero.[5] To demonstrate this point explicitly, in Fig. 3-b we again display the $\overline{MS}$ ZM-VFNS and the ACOT results but this time with a logarithmic scale to highlight the small m region. We clearly see that ACOT reduces the $\overline{MS}$ ZM-VFNS exactly in this limit without any additional finite renormalization contributions.[6]

---

[5] If we were to compute this process in the $\overline{MS}$ scheme, the $\ln(m^2/Q^2)$ in the SUB term would simply be replaced by a $1/\varepsilon$ pole which would cancel the corresponding singularity in the NLO contribution.

[6] It is possible to define other massive schemes that could include additional matching parameters or extra observable–dependent contributions. For example, the calculation of F_2^c in the original RT scheme [7] included extra higher-order contributions that do not vanish as $Q/m \to \infty$.
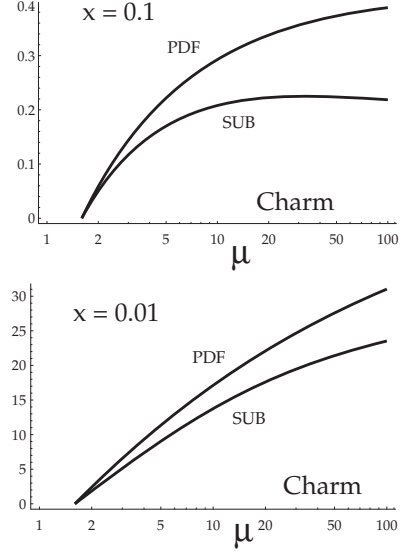

Figure 4: Comparison of the DGLAP evolved charm PDF $f_c(x, \mu)$ with the perturbatively computed single splitting (SUB) $\widetilde{f}_c(x, \mu) = f_g(x, \mu) \otimes \widetilde{P}_{g \to c}$ vs. μ in GeV for two representative values of x.

The ACOT scheme is minimal in the sense that the construction of the massive short distance cross sections does not need any observable–dependent extra contributions or any regulators to smooth the transition between the high and low scale regions. The ACOT prescription is to just calculate the massive partonic cross sections and perform the factorization using the quark mass as regulator.

It is in this sense that we claim the ACOT scheme is the minimal massive extension of the $\overline{MS}$ ZM-VFNS. In the limit $m/\mu \to 0$ it reduces exactly to the $\overline{MS}$ ZM-VFNS, in the limit $m/\mu \gtrsim 1$ the heavy quark decouples from the PDFs and we obtain exactly the FFNS for $m/\mu \gg 1$ and no finite renormalizations or additional parameters are needed.

4. When do we need Heavy Quark PDFs

The novel ingredient in the above calculation is the inclusion of the heavy quark PDF contribution which resums logs of $\alpha_S \ln(\mu^2/m^2)$. An obvious question is when do we need to consider such terms, and how large are their contributions? The answer is illustrated in Fig. 4 where we compare the DGLAP evolved PDF $f_Q(x, \mu)$ with the single splitting perturbative result $\widetilde{f}_Q(x, \mu)$.

The DGLAP PDF evolution sums a non-perturbative infinite tower of logs which are contained in σ_{LO} while the σ_{SUB} contribution removes the perturbative single splitting component which is already included in the σ_{NLO} contribution. Hence, at the PDF level the differ-
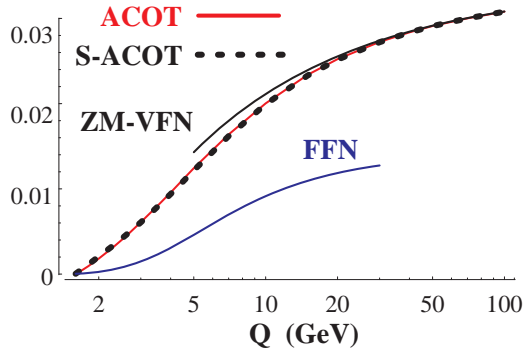
Figure 5: F_2^c for $x = 0.1$ for NLO DIS heavy quark production as a function of Q. We display calculations using the ACOT, S-ACOT, Fixed-Flavor Number Scheme (FFNS), and Zero-Mass Variable Flavor Number Scheme (ZM-VFNS). The ACOT and S-ACOT results are virtually identical.

ence between the heavy quark DGLAP evolved PDF f_Q and the single-splitting perturbative $\tilde{f}_Q$ will indicate the contribution of the higher order logs which are resummed into the heavy quark PDF. Here, $\tilde{f}_Q = f_g \otimes \tilde{P}_{g\to Q}$ represents the PDF of a heavy quark Q generated from a single perturbative splitting.

For $\mu \sim m$ we see that f_Q and $\tilde{f}_Q$ match quite closely, whereas they differ significantly for μ values a few times m. While the details will depend on the specific process, in general we find that for μ-scales a few times m the terms resummed by the heavy quark PDF can be significant. Additionally, the difference between f_Q and $\tilde{f}_Q$ will be reduced at higher orders as more perturbative splittings are included in $\tilde{f}_Q$.

Note that these scales are much lower than one might estimate using the naive criterion $\frac{\alpha_S}{2\pi} \ln(\mu^2/m^2) \sim 1$; in particular, the ACOT calculation often yields reduced μ-dependence as the quark dominated σ_{LO} contributions typically have behavior which is complementary to the gluon-initiated σ_{NLO} terms.

B. S-ACOT

In a corresponding application, it was observed that the heavy quark mass could be set to zero in certain pieces of the hard scattering terms without any loss of accuracy. This modification of the ACOT scheme goes by the name Simplified-ACOT (S-ACOT) and can be summarized as follows [8].

S-ACOT: For hard-scattering processes with incoming heavy quarks or with internal on-shell cuts on a heavy quark line, the heavy quark mass can be set to zero ($m = 0$) for these pieces.

If we consider the case of NLO DIS heavy quark production, this means we can set $m = 0$ for the LO terms ($QV \to Q$) as this involves an incoming heavy quark, and we can set $m = 0$ for the SUB terms as this has an on-shell cut on an internal heavy quark line. Hence, the only contribution which requires calculation with m retained is the NLO $gV \to Q\bar{Q}$ process. Figure 5 displays a comparison of a calculation using the ACOT scheme with all masses retained vs. the S-ACOT scheme; as expected, these two results match throughout the full kinematic region.

It is important to note that the S-ACOT scheme is not an approximation; this is an exact renormalization scheme, extensible to all orders.

C. ACOT and χ-Rescaling

As we have illustrated in Sec. II A above, in the limit $Q^2 \gg m^2$ the mass simply plays the role of a regulator. In contrast, for $Q^2 \sim m^2$ the value of the mass is of consequence for the physics. The mass can enter dynamically in the hard-scattering matrix element, and can enter kinematically in the phase space of the process.

We will demonstrate that for the processes of interest the primary role of the mass is kinematic and not dynamic. It was this idea which was behind the original slow-rescaling prescription of [9] which considered DIS charm production (e.g., $\gamma c \to c$) introducing the shift

$$x \to \chi = x \left[1 + \left(\frac{m_c}{Q}\right)^2\right]. \quad (3)$$

This prescription accounted for the charm quark mass by effectively reducing the phase space for the final state by an amount proportional to $(m_c/Q)^2$.

This idea was extended in the χ-scheme by realizing that in addition to the observed final-state charm quark, if the beam has a charm-flavor quantum number of zero (such as a proton beam) then there is also an anti-charm quark in the beam fragments because all the charm quarks are ultimately produced by gluon splitting ($g \to c\bar{c}$) into a charm pair.[7] For this case the scaling variable becomes

$$\chi = x \left[1 + \left(\frac{2m_c}{Q}\right)^2\right]. \quad (4)$$

[7] If the beam has non-zero charm-flavor quantum number, such as a D-meson, this argument would be incorrect. Technically, χ-scaling violates factorization as we are presuming the mass of the beam fragments; if we perform a thought experiment with a beam of D-mesons, charm quark need not be associated with an anti-charm quark.

This rescaling is implemented in the ACOT_χ scheme, for example [10–12]. The factor $(1 + (2m_c)^2/Q^2)$ represents a kinematic suppression factor which will suppress the charm process relative to the lighter quarks. Additionally, the χ-scaling ensures the threshold kinematics $(W^2 > 4m_c^2 + M^2)$ are satisfied; while it is important to satisfy this condition for large x, this may prove too restrictive at small x where the HERA data are especially precise.[8]

To encompass all the above results, we can define a general scaling variable $\chi(n)$ as

$$\chi(n) = x \left[1 + \left(\frac{n\, m_c}{Q} \right)^2 \right] \qquad (5)$$

where $n = \{0, 1, 2\}$. Here, $n = 0$ corresponds to the massless result without rescaling, $n = 1$ corresponds to the original Barnett slow-rescaling, and $n = 2$ corresponds to the χ-rescaling.

D. Phase Space (Kinematic) & Dynamic Mass

We now investigate the effects of separately varying the mass entering the $\chi(n)$ variable taking into account the phase space constraints and the mass value entering the hard scattering cross section $\hat\sigma(m)$. We call the former mass parameter "phase space (kinematic) mass" and the latter "dynamic mass"[9].

In Fig. 6a we display $F_2^c(x, Q)$ vs. Q. The family of 3 curves shows the NLO ACOT calculation with $\chi(n)$ scaling using a zero dynamic mass for the hard scattering. We compare this with Fig. 6b which shows $F_2^c(x, Q)$ in the NLO ACOT scheme using a fixed $n = 2$ scaling, but varying the mass used in the hard-scattering cross section. The upper (cyan) curves use a non-zero dynamic mass $[\hat\sigma(m_c = 1.3)]$ and the lower (purple) curves have been obtained with a vanishing dynamic mass $[\hat\sigma(m_c = 0)]$. We observe that the effect of the 'dynamic mass' in $\hat\sigma(m_c)$ is only of consequence in the limited region $Q \gtrsim m$, and even in this region the effect is minimal. In contrast, the influence of the phase space (kinematic) mass shown in Fig. 6a is larger than the dynamic mass shown in Fig. 6b. To highlight these differences, we scale the curves in Fig. 7 by the massless $n = 2$ scaling result and plot bands that represent the variation of the dynamic and kinematic masses.

In conclusion, we have shown that (up to $\mathcal{O}(\alpha_S)$) the phase space mass dependence is generally the dominant contribution to the DIS structure functions. Assuming that this observation remains true at higher orders, it is possible to obtain a good approximation of the structure functions in the ACOT scheme at NNLO and N³LO using the massless Wilson coefficients together with a non-zero phase space mass entering via the $\chi(n)$-prescription.

III. ACOT SCHEME BEYOND NLO

We have shown using the NLO full ACOT scheme that the dominant mass effects are those coming from the phase space which can be taken into account via a generalized slow-rescaling $\chi(n)$-prescription. Assuming that a similar relation remains true at higher orders, one can construct the following approximation to the ACOT result up to N³LO ($\mathcal{O}(\alpha_S^3)$):

$$\begin{aligned} \text{ACOT}[\mathcal{O}(\alpha_S^{0+1+2+3})] \; &\simeq \\ \text{ACOT}[\mathcal{O}(\alpha_S^{0+1})] &+ \text{ZM-VFNS}_{\chi(n)}[\mathcal{O}(\alpha_S^{2+3})] \end{aligned} \qquad (6)$$

In this equation, "ACOT" generically represents any variant of the ACOT scheme (ACOT, S-ACOT, S-ACOT$_\chi$); for the results presented in Sec. IV, we will use the fully massive ACOT scheme with all masses retained out to NLO. The ZM-VFNS$_{\chi(n)}$ term uses the massless Wilson coefficients at $\mathcal{O}(\alpha\,\alpha_S^2)$ and $\mathcal{O}(\alpha\,\alpha_S^3)$ with the specified $\chi(n)$-scaling.[10] Sample processes which contribute at this order are displayed in Fig. 8.

We use the ZM-VFNS$_{\chi(n)}$ result in Eq. (6) to approximate the higher-order terms because not all the necessary massive Wilson coefficients at $\mathcal{O}(\alpha\,\alpha_S^2)$ and $\mathcal{O}(\alpha\,\alpha_S^3)$ have been computed. There has been a calculation of neutral current electroproduction (equal quark masses, vector coupling) of heavy quarks at this order by Smith & VanNeerven [13] in the FFNS which could be used to obtain the massive Wilson coefficients in the S-ACOT scheme by applying appropriate collinear subtraction terms. However, for the original ACOT scheme it would then still be necessary to compute the massive Wilson coefficients for the heavy quark initiated subprocess at $\mathcal{O}(\alpha\,\alpha_S^2)$. See Refs. [12, 14] for details.

Using the result of Ref. [13], Thorne and Roberts developed an NLO VFNS [7, 15], and an improved NNLO formulation was presented in Ref. [16]. The FONLL formalism was outlined in Ref. [17] and this was used to construct matched expressions for structure functions to NNLO [18]; implications of these results in the context of the NNPDF analysis were presented in Ref. [19].

---

[8] We sketch the relevant kinematics in Appendix A 3.

[9] Note that the finite mass terms $(m^2/Q^2)^n$ in $\hat\sigma(m)$ receive contributions from both, masses in the heavy quark propagators and masses in the phase space. Still we refer to them as dynamic mass terms and show that they are numerically less important than the mass terms in the slow rescaling variable $\chi(n)$ which are of purely kinematic origin.

[10] In Sec.II.A.2 we demonstrated that the ACOT calculation reduces to the ZM-VFNS result in the massless limit. We will address the choice of the $\chi(n)$-rescaling in the Sec. III.A.
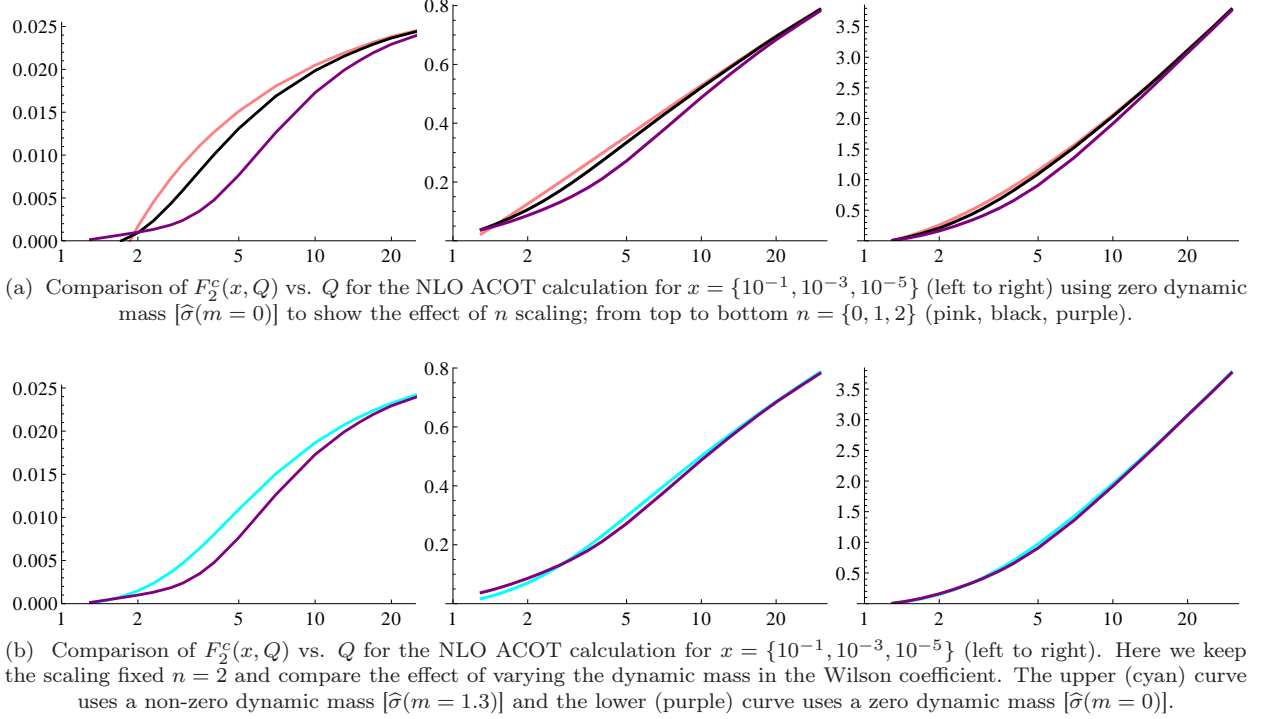
(a) Comparison of $F_2^c(x, Q)$ vs. Q for the NLO ACOT calculation for $x = \{10^{-1}, 10^{-3}, 10^{-5}\}$ (left to right) using zero dynamic mass $[\hat{\sigma}(m = 0)]$ to show the effect of n scaling; from top to bottom $n = \{0, 1, 2\}$ (pink, black, purple).

(b) Comparison of $F_2^c(x, Q)$ vs. Q for the NLO ACOT calculation for $x = \{10^{-1}, 10^{-3}, 10^{-5}\}$ (left to right). Here we keep the scaling fixed $n = 2$ and compare the effect of varying the dynamic mass in the Wilson coefficient. The upper (cyan) curve uses a non-zero dynamic mass $[\hat{\sigma}(m = 1.3)]$ and the lower (purple) curve uses a zero dynamic mass $[\hat{\sigma}(m = 0)]$.

Figure 6: Comparison of phase space (kinematic) & dynamic mass effects
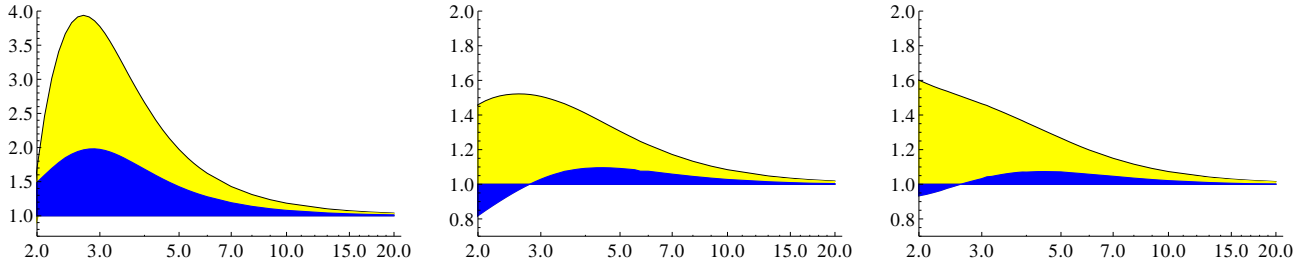

Figure 7: Comparison of kinematic & dynamic mass effects for $F_2^c(x, Q)$ vs. Q for the NLO ACOT calculation for $x = \{10^{-1}, 10^{-3}, 10^{-5}\}$ (left to right). The curves are scaled by the massless $n = 2$ result. The wider (yellow) band represents the variation of the kinematic mass of Fig. 6a; note this band extends down to a ratio of 1.0. The narrower (blue) band is overlaid on the plot and represents the variation of the dynamic mass of Fig. 6b.

An overview and comparison of these analyses was presented in the 2009 Les Houches report [20]. More recently, an NNLO S-ACOT-χ calculation was developed in Refs. [12, 14]. For charge current case massive calculations are available at order $\mathcal{O}(\alpha \alpha_S)$ [21–23] and partial results at order $\mathcal{O}(\alpha \alpha_S^2)$ [24]. Comparative analyses of these schemes are under investigation; however, this is beyond the scope of this paper.

Here, we argue that the massless Wilson coefficients at $\mathcal{O}(\alpha \alpha_S^2)$ together with a $\chi(n)$-prescription provide a very good approximation of the exact result. At worst, the maximum error would be of order $\mathcal{O}(\alpha \alpha_S^2 \times [m^2/Q^2])$. However, based on the arguments of Sec. II D we expect the inclusion of the phase space mass effects to contain the dominant higher order contributions so that the ac-

tual error should be substantially smaller.

The massless higher order coefficient functions for the DIS structure function F_2 via photon exchange can be found in Refs. [25–27] for $\mathcal{O}(\alpha_S^1)$, Refs. [28–30] for $\mathcal{O}(\alpha_S^2)$, and Ref. [31] for $\mathcal{O}(\alpha_S^3)$. For our numerical code we have used the x-space parameterization provided in Refs. [32, 33] for $\mathcal{O}(\alpha_S^2)$, and Refs. [31, 34] for $\mathcal{O}(\alpha_S^3)$.

The expressions for the structure function F_L have been calculated in Refs. [29, 35] for $\mathcal{O}(\alpha_S^2)$, and Ref. [31] for $\mathcal{O}(\alpha_S^3)$. In our FORTRAN code we have used the x-space parameterization provided in Refs. [32, 36] for $\mathcal{O}(\alpha_S^2)$ and Ref. [36] for $\mathcal{O}(\alpha_S^3)$.

In order to calculate the inclusive structure functions F_2 and F_L in the ZM-VFNS$_\chi$ using these Wilson coefficients, plus- and delta-distributions have to be evaluated
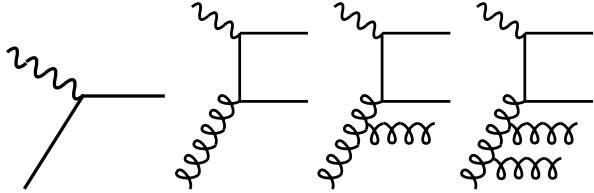
Figure 8: Sample Feynman diagrams contributing to DIS heavy quark production (from left): LO $\mathcal{O}(\alpha_S^0)$ quark-boson scattering $QV \to Q$, NLO $\mathcal{O}(\alpha_S^1)$ gluon-boson scattering $gV \to Q\bar{Q}$, NNLO $\mathcal{O}(\alpha_S^2)$ boson-gluon scattering $gV \to gQ\bar{Q}$, and N^{3}LO $\mathcal{O}(\alpha_S^3)$ boson-gluon scattering $gV \to ggQ\bar{Q}$.

which is in principle straightforward. However, for the implementation of the slow-rescaling prescription it is necessary to decompose the Wilson coefficients into the contributions from different parton flavors. This step is non-trivial at $\mathcal{O}(\alpha_S^2)$ and beyond, and we therefore provide some details of our calculation in the Appendix B.

A. Choice of $\chi(n)$-Rescaling

We now consider our choice for the appropriate generalized $\chi(n)$-rescaling variable.

In Table I we display the various rescalings of ξ for the LO $\gamma Q \to Q$ process and the NLO $\gamma g \to Q\bar{Q}$ process. The "general" result is obtained by working out the detailed kinematics for the corresponding process [37].

The factor η is the rescaling due to the hadronic mass M; notice that this factors out from the partonic mass dependence as it should [1]. For details see Appendix A.

The LO case with full massive kinematics has been computed in Ref. [37]. In the limit where the initial mass is small ($m_1 \to 0$), we recover the Barnett [9] slow-rescaling result. Additionally, we obtain the curious result that for a neutral current equal mass case ($m_1 = m_2$) the rescaling is this same factor.

For the NLO gluon-induced process, the interpretation of the rescaling is straightforward; the phase space is simply suppressed by the total invariant mass of the final state ($m_1 + m_2$) compared to the scale Q. For the charged current case where we neglect m_1, we again obtain the standard rescaling factor. However, for the neutral current case ($m_1 = m_2$) we obtain a rescaling factor which is analogous to the χ-scaling factor.

For the purposes of this study, we will vary the phase space mass using the $\chi(n)$ rescaling with $n = \{0, 1, 2\}$. While $n = 0$ corresponds to the massless case (no rescaling), it is not obvious whether $n = 1$ or $n = 2$ is the preferred rescaling choice for higher orders. Thus, we will use the range between $n = 1$ and $n = 2$ as a measure of our theoretical uncertainty arising from this ambiguity.

IV. RESULTS

We now present the results of our calculation extending the ACOT scheme to NNLO and N^{3}LO. As outlined in Eq. (6), we will use the fully massive ACOT scheme for the LO and NLO contributions, and combine this with the ZM-VFNS supplemented with the χ-rescaling prescription to approximate the higher order terms. We will use the QCDNUM program [38] with the VFNS evolved with the DGLAP kernels at NNLO to generate our PDFs from an initial distribution based on the Les Houches benchmark set [39]; this ensures that our heavy quark PDFs are consistently evolved so that the heavy quark initiated LO terms properly match the corresponding SUB contribution. At NNLO the proper matching conditions across flavor thresholds introduces discontinuities in the PDFs which are incorporated in the QCDNUM program; we discuss this in detail in Appendix C. We choose $m_c = 1.3$ GeV, $m_b = 4.5$ GeV, $\alpha_S(M_Z) = 0.118$. We note that the QCDNUM ZM-STFN package has the massless Wilson coefficients computed up to N^{3}LO; we cross checked our implementation of ACOT in the massless limit with QCDNUM, and they agree precisely.

A. Effect of $\chi(n)$-Scaling

In Figures 9a and 9b we display the structure functions F_2 and F_L, respectively, for selected x values as a function of Q. Each plot has three curves which are computed using n-scalings of $\{0, 1, 2\}$. We observe that the effect of the n-scaling is negligible except for very small Q values. This result is in part because the heavy quarks are only a fraction of the total structure function, and the effects of the n-scaling are reduced at larger Q values.

In Fig. 10 we magnify the small Q region of F_L of Fig. 9b for $x = 10^{-5}$, where the effects of using different scalings are largest. We can see that for inclusive observables, the $n = 1$ and $n = 2$ scalings give nearly identical results, but they differ from the massless case ($n = 0$). This result, together with the observation that at NLO kinematic mass effects are dominant, suggests that the error we have in our approach is relatively small and approximated by the band between $n = 1$ and $n = 2$ results.

B. Flavor Decomposition of $\chi(n)$ Scaling

We can investigate the effects of the $\chi(n)$-scaling in more details by examining the flavor decomposition of the structure functions.

In Figures 11a and 11b we display the fractional contributions of quark flavors to the structure functions $F_{2,L}$

ξ	General	$m_1 = 0$	$m_1 = m_2 = m$	χ-scheme:
	$\eta\left[\dfrac{Q^2-m_1^2+m_2^2+\Delta[-Q^2,m_1^2,m_2^2]}{2Q^2}\right]$	$\eta\left[1+\dfrac{m_2^2}{Q^2}\right]$	$\eta\left[1+\dfrac{m^2}{Q^2}\right]$	$\eta\left[1+\dfrac{(2m)^2}{Q^2}\right]$
	$\eta\left[1+\left(\dfrac{m_1+m_2}{Q}\right)^2\right]$	$\eta\left[1+\dfrac{m_2^2}{Q^2}\right]$	$\eta\left[1+\dfrac{(2m)^2}{Q^2}\right]$	$\eta\left[1+\dfrac{(2m)^2}{Q^2}\right]$

Table I: The massive rescaling factor for the LO quark-initiated process ($Vq_1 \to q_2$), and the NLO gluon-initiated process ($Vg \to q_1\overline{q}_2$). The quarks $q_{1,2}$ have mass $m_{1,2}$, respectively, and V represents the vector boson; γ/Z for neutral current processes ($m_1 = m_2$), and $W^\pm$ for charged current processes ($m_1 \neq m_2$). η is the scaling factor which depends on the hadronic mass M; see Appendix A for details. The triangle-function is defined as:
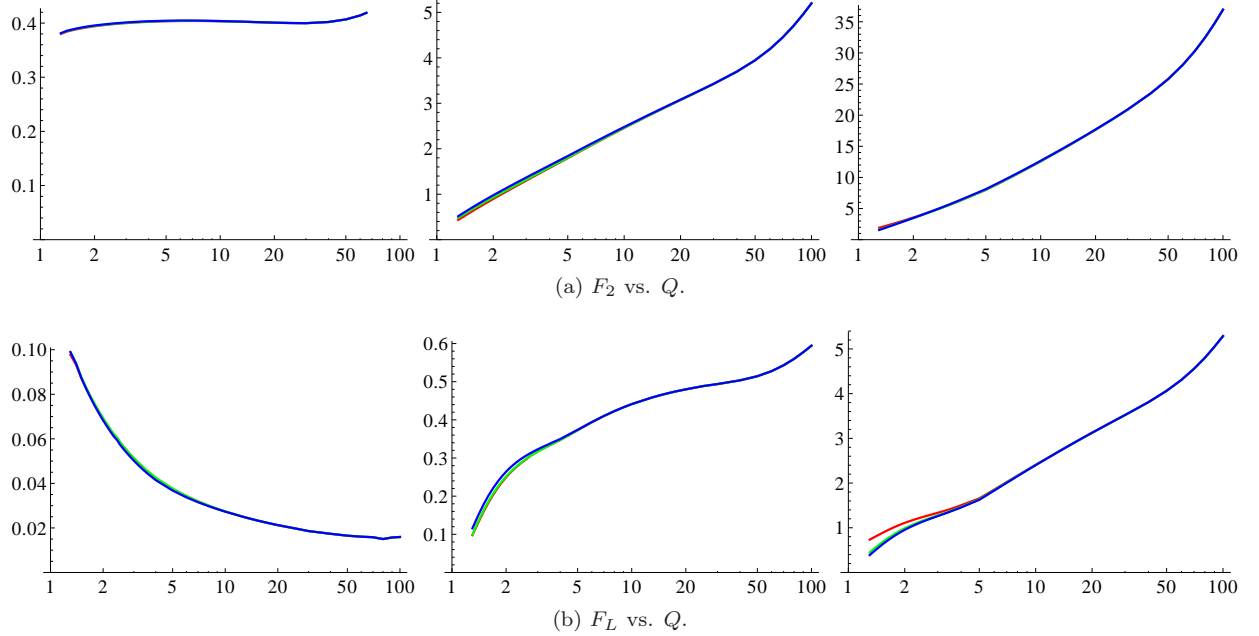$$\Delta[a,b,c] = \sqrt{a^2 + b^2 + c^2 - 2(ab + bc + ca)}.$$

(a) F_2 vs. Q.

(b) F_L vs. Q.

Figure 9: $F_{2,L}$ vs. Q at N^{3}LO for fixed $x = \{10^{-1}, 10^{-3}, 10^{-5}\}$ (left to right). The three lines show the scaling variable: $n = \{0, 1, 2\}$ (red, green, blue). We observe the effect of the n-scaling is negligible except for very small Q values.
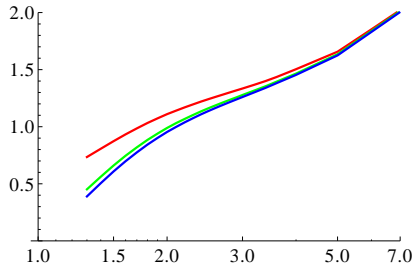

Figure 10: Enlargement of Fig. 9b for $x = 10^{-5}$ showing the small Q region. Here we can distinguish plots for different scalings; from top to bottom we have $n = \{0, 1, 2\}$ (red, green, blue).

for selected n-scaling values as a function of Q. Flavor decomposition of inclusive structure functions is defined in appendix B in Eqs. (B1) and (B2). We observe the n-scaling reduces the relative contributions of charm and bottom at low Q scales. For example, without any n-scaling ($n = 0$) we find the charm and bottom quarks contribute an unusually large fraction at very low scales ($Q \sim m_c$) as they are (incorrectly) treated as massless partons in this region. The result of the different n-scalings ($n = 1, 2$) is to introduce a kinematic penalty which properly suppresses the contribution of these heavy quarks in the low Q region. In the following, we will generally use the $n = 2$ scaling for our comparisons.

C. $F_{2,L}$ Initial-State Flavor Decomposition

In Figures 12a and 12b we display the fractional contributions for the initial-state quarks (i) to the structure
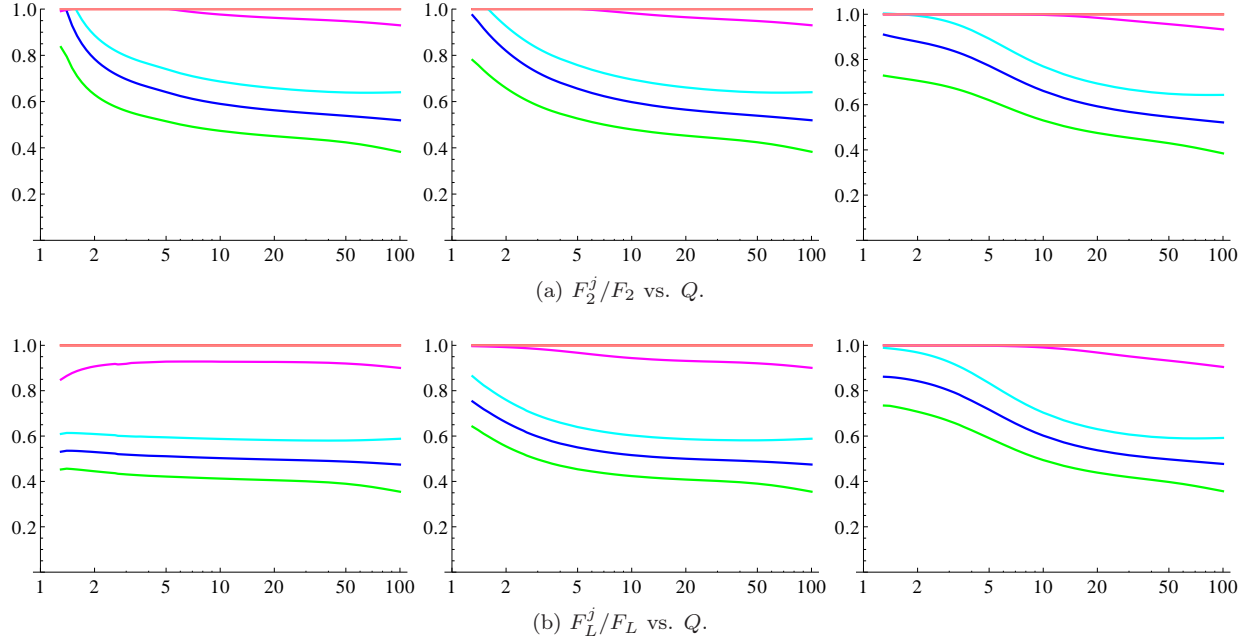
(a) F_2^j/F_2 vs. Q.

(b) F_L^j/F_L vs. Q.

Figure 11: Effect of $\chi(n)$-scaling for $n = \{0, 1, 2\}$ (left to right) at N^{3}LO for fixed $x = \{10^{-3}\}$. Reading from the bottom we have fractional contribution for each quark flavor to $F_{2,L}^j/F_{2,L}$ vs. Q from $\{u, d, s, c, b\}$ (green, blue, cyan, magenta, pink).

functions F_2 and F_L,[11] respectively, for selected x values as a function of Q; here we have used $n = 2$ scaling. Reading from the bottom, we have the cumulative contributions from the $\{g, u, d, s, c, b\}$. Although this decomposition is not physically observable, it is instructive to see which PDFs are dominantly influencing the result. We observe that for large x and low Q the heavy flavor contributions are minimal. For example, for $x = 10^{-1}$ we see the contribution of the u-quark comprises $\sim 80\%$ of the F_2 structure function at low Q. In contrast, at $x = 10^{-5}$ and large Q we see the F_2 contributions of the u-quark and c-quark are comparable (as they both couple with a factor $4/9$), and the d-quark and s-quark are comparable (as they both couple with a factor $1/9$).

It is notable that the gluon contribution to F_L is significant. For $x = 10^{-1}$ this is roughly 40% throughout the Q range, and can be even larger for smaller x values.

D. $F_{2,L}$ Final-State Flavor Decomposition

In Figures 13a and 13b we display the fractional contributions for the final-state quarks (j) to the structure functions F_2 and F_L, respectively, for selected x values as a function of Q; here we have used $n = 2$ scaling. Reading from the bottom, we have the cumulative contributions from the $\{u, d, s, c, b\}$. Again, we observe that for large x and low Q the heavy flavor contributions are minimal, but these can grow quickly as we move to smaller x and larger Q.

E. Comparison of LO, NLO, NNLO, N^{3}LO

In Figure 14a we display the results for F_2 vs. Q computed at various orders. For large x (c.f. $x = 0.1$) we find the perturbative calculation is particularly stable; we see that the LO result is within 20% of the others at small Q, and within 5% at large Q. The NLO is within 2% at small Q, and indistinguishable from the NNLO and N^{3}LO for Q values above ~ 10 GeV. The NNLO and N^{3}LO results are essentially identical throughout the kinematic range. For smaller x values (10^{-3}, 10^{-5}) the contribution of the higher order terms increases. Here, the NNLO and N^{3}LO coincide for Q values above ~ 5 GeV, but the NLO result can differ by $\sim 5\%$.

In Figure 14b we display the results for F_L vs. Q computed at various orders. In contrast to F_2, we find the NLO corrections are large for F_L; this is because the LO F_L contribution (which violates the Callan-Gross relation) is suppressed by (m^2/Q^2) compared to the dominant gluon contributions which enter at NLO. Consequently, we observe (as expected) that the LO result for F_L receives large contributions from the higher or-

---

[11] Fractional decomposition of "initial-state" structure functions is understood as $F_{2,L}^i = \sum_{j=1}^{6} F_{2,L}^{ij}$.
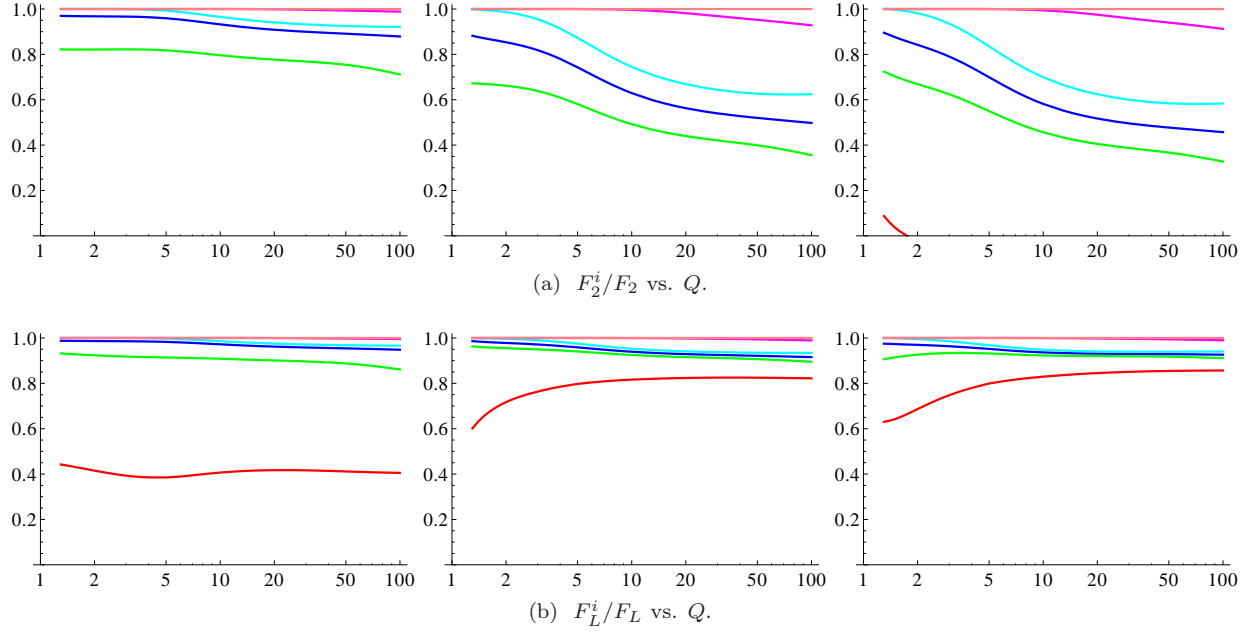
(a) F_2^i/F_2 vs. Q.

(b) F_L^i/F_L vs. Q.

Figure 12: Fractional flavor decomposition of "initial-state" $F_{2,L}^i/F_{2,L}$ vs. Q at N³LO for $x = \{10^{-1}, 10^{-3}, 10^{-5}\}$ (left to right) for $n = 2$ scaling. Reading from the bottom, we plot the cumulative contributions to $F_{2,L}$ from $\{g, u, d, s, c, b\}$, (red, green, blue, cyan, magenta, pink).

der terms.[12] Essentially, the NLO is the first non-trivial order for F_L, and the subsequent contributions then converge. For example, at large x (c.f. $x = 0.1$) for $Q \sim 10$ GeV we find the NLO result yields ~ 60 to 80% of the total, the NNLO is a $\sim 20\%$ correction, and the N³LO is a $\sim 10\%$ correction. For lower x values (10^{-3}, 10^{-5}) the convergence of the perturbative series improves, and the NLO results is within $\sim 10\%$ of the N³LO result. Curiously, for $x = 10^{-5}$ the NNLO and N³LO roughly compensate each other so that the NLO and the N³LO match quite closely for $Q \geq 2$ GeV.

While the calculation of F_L is certainly more challenging, examining Fig. 1 we see that for most of the relevant kinematic range probed by HERA the theoretical calculation is quite stable. For example, in the high Q^2 region where HERA is probing intermediate x values ($x \sim 10^{-3}$) the spread of the $\chi(n)$ scalings is small. The challenge arises in the low Q region ($Q \sim 2$ GeV) where the x values are $\sim 10^{-4}$; in this region, there is some spread between the various curves at the lowest x value ($\sim 10^{-5}$), but for $x \sim 10^{-3}$ this is greatly reduced.

V. CONCLUSIONS

We extended the ACOT calculation for DIS structure functions to N³LO by combining the exact ACOT scheme at NLO with a $\chi(n)$-rescaling; this allows us to include the leading mass dependence at NNLO and N³LO. Using the full ACOT calculation at NLO, we demonstrated that the heavy quarks mass dependence for the DIS structure functions is dominated by the kinematic mass contributions, and this can be implemented via a generalized $\chi(n)$-rescaling prescription.

We studied the F_2 and F_L structure functions as a function of x and Q. We examined the flavor decomposition of these structure functions, and verified that the heavy quarks were appropriately suppressed in the low Q region. We found the results for F_2 were very stable across the full kinematic range for $\{x, Q\}$, and the contributions from the NNLO and N³LO terms were small. For F_L, the higher order terms gave a proportionally larger contribution (due to the suppression of the LO term from the Callan-Gross relation); nevertheless, the contributions from the NNLO and N³LO terms were generally small in the region probed by HERA.

The result of this calculation was to obtain precise predictions for the inclusive F_2 and F_L structure functions which can be used to analyze the HERA data.

---

[12] Because we use the fully massive ACOT scheme to LO and NLO, the LO result in Fig. 14b contains the (m^2/Q^2) helicity-violating contributions $\sim \mathcal{O}(\alpha_s^0)$; hence, it is non-zero. In the S-ACOT scheme, the LO result for F_L vanishes, but the NLO result is comparable to the NLO ACOT result.
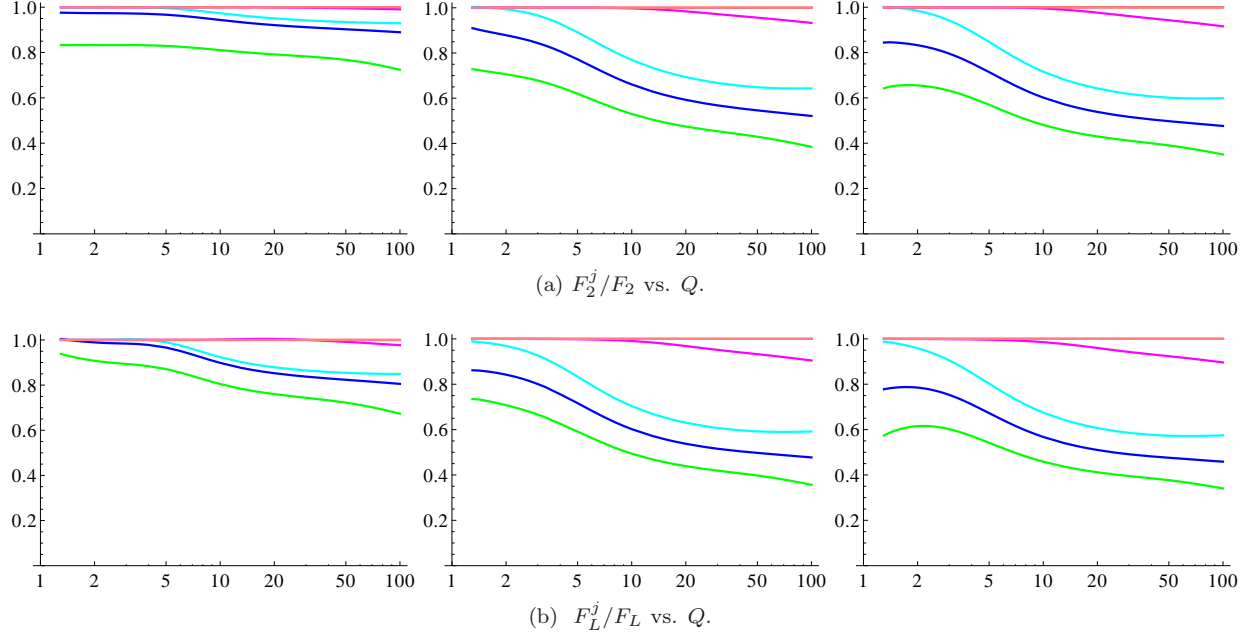
(a) F_2^j/F_2 vs. Q.

(b) F_L^j/F_L vs. Q.

Figure 13: Fractional contribution for each quark flavor to $F_{2,L}^j/F_{2,L}$ vs. Q at N³LO for fixed $x = \{10^{-1}, 10^{-3}, 10^{-5}\}$ (left to right). Results are displayed for $n = 2$ scaling. Reading from the bottom, we have the cumulative contributions from the $\{u, d, s, c, b\}$ (green, blue, cyan, magenta, pink).
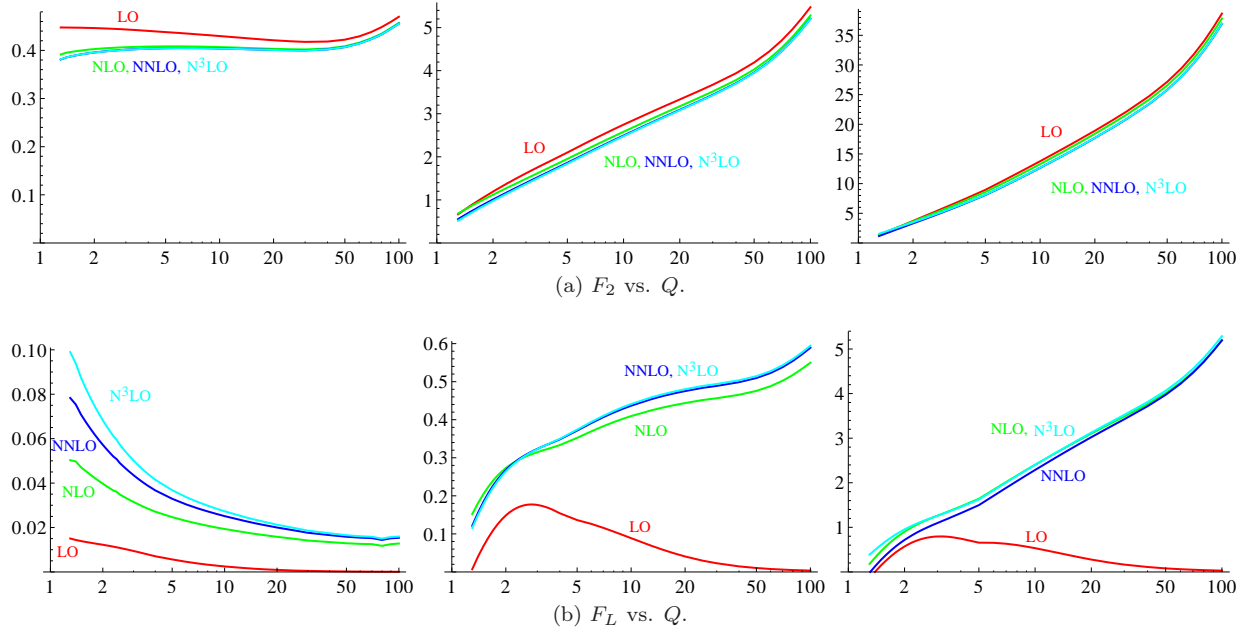

(a) F_2 vs. Q.

(b) F_L vs. Q.

Figure 14: $F_{2,L}$ vs. Q at $\{$LO, NLO, NNLO, N³LO$\}$ (red, green, blue, cyan) for fixed $x = \{10^{-1}, 10^{-3}, 10^{-5}\}$ (left to right) for $n = 2$ scaling.

Appendix A: Kinematic Relations

1. Target Mass Contributions

In the DIS process, the effect of the target mass (M) on the scaling variable is a multiplicative correction fac-tor

$$\eta = \frac{2x}{1 + \sqrt{1 + \frac{4x^2 M^2}{Q^2}}}$$

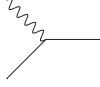$$\xrightarrow[M \to 0]{} x\left[1 - \left(\frac{xM}{Q}\right)^2\right] + \dots \quad . \tag{A1}$$

Figure 15: $\mathcal{O}(\alpha_S^0)$ - $\gamma^* q_i \to q_i$. Contributes to $C_{a,q}^{\mathrm{ns}}$ (and hence to $C_{a,q}^{\mathrm{s}}$) but not to $C_{a,q}^{\mathrm{ps}}$.

Figure 16: $\mathcal{O}(\alpha_S^1)$ - $\gamma^* q_i \to q_i g$. Contributes to $C_{a,q}^{\mathrm{ns}}$ (and hence to $C_{a,q}^{\mathrm{s}}$) but not to $C_{a,q}^{\mathrm{ps}}$. This contribution does not depend on n_f.

Figure 17: $\mathcal{O}(\alpha_S^1)$ - $\gamma^* g \to q_j \bar{q}_j$.

This is used in Table I to modify the scaling variable [1, 37].

2. Barnett Scaling

If we consider the charged-current DIS process for charm production, this takes place via the subprocess $W^+(q)\, s(\xi P) \to c(k)$. If we impose 4-momentum conservation, we have $(q + \xi P)^2 = k^2 = m_c^2$. Defining $q^2 = -Q^2$ and $x = Q^2/(2p \cdot q)$, we obtain the traditional "slow rescaling" relation [9]

$$\xi = x \left(1 + \frac{m_c^2}{Q^2}\right)$$

which was used in Eq. (3).

3. $\widehat{W}$ constraints

If we compute the invariant mass $\widehat{W}$ of a boson of momentum q scattering from a light parton a of momentum $p_a = \xi P$, we find [14]

$$\widehat{W} = (p_a + q)^2 = Q^2(\xi/x - 1) \quad . \qquad (A2)$$

If the partonic final state has a minimum invariant mass $\widehat{W}_{min} = 4m^2$, then ξ is constrained by

$$1 \geq \xi \geq \chi \geq x \qquad (A3)$$

where $\chi = x(1 + 4m^2/Q^2)$. This is the relation used in Eq. (4). This choice will ensure $\widehat{W} \geq \widehat{W}_{min}$ is satisfied. While this constraint is important in the large x region, this may be too restrictive in the small x region—especially as this is the region where the HERA data is very precise.

Appendix B: Decomposition of the Wilson coefficients

In this appendix we present the decomposition of the Wilson coefficients used to implement the scheme. We will need to decompose the structure function F in terms of the individual partonic contributions,

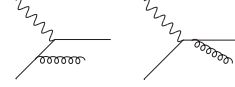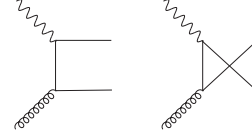$$F = \sum_{i=0}^{5} \sum_{j=1}^{6} F^{ij} \qquad (B1)$$

where the indices i and j represent initial and final-state partons respectively (see captions of Figs. 15–24). More specifically, $i = 0$ denotes a gluon and $i, j = 1, 2, 3, \ldots$ denotes u, d, s, $\ldots$ quarks and anti-quarks. A top quark PDF ($i = 6$) is not included in this study.

Let us consider the heavy quark structure functions $F_{2,L}^c$ as an example. This is obtained by requiring that there is a charm in the initial state while summing over the final-state flavors up to and including charm in Eq. (B1), or by requiring that there is a charm in the final-state and summing over the initial flavors up to and including charm. Thus, we obtain:

$$F^c = \sum_{i=0}^{3} F^{i4} + \sum_{j=1}^{3} F^{4j} + F^{44} \quad . \qquad (B2)$$

The case where the initial and final-state are both charm quarks (F^{44}) has been written explicitly in the equation to avoid double counting this contribution.[13] The first sum in Eq. (B2) includes cases, as in Fig. 20, where the incoming quark is a light quark while the charm quark is one of the quarks in the quark anti-quark pair.

In order to obtain the required decomposition, there are some manipulations that need to be performed to transform from the singlet (s), non-singlet (ns), and purely-singlet (ps) structure function combinations found in the literature into individual partonic components.

The general expression for the structure function is given by:

$$x^{-1} F_a = q_{ns} \otimes C_{a,q}^{\mathrm{ns}} + \langle e^2 \rangle \left(q_s \otimes C_{a,q}^{\mathrm{s}} + g \otimes C_{a,g}\right) \qquad (B3)$$

---

[13] Note that in our decomposition, diagrams with a bottom quark in the initial or final state, contribute to the bottom structure function, even in the presence of a charm quark.
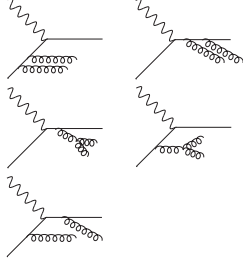
Figure 18: $\mathcal{O}(\alpha_S^2)$ - $\gamma^* q_i \to q_i gg$. Contributes to $C_{a,q}^{\mathrm{ns}}$ (and hence to $C_{a,q}^{\mathrm{s}}$) but not to $C_{a,q}^{\mathrm{ps}}$. This part is independent of n_f.
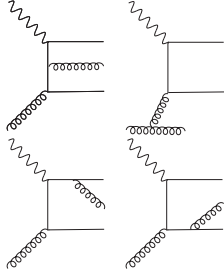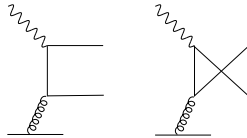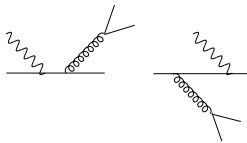

Figure 19: $\mathcal{O}(\alpha_S^2)$ - $\gamma^* g \to q_j \bar{q}_j g$.

(a) Contribution proportional to n_f for $C_{a,q}^{\mathrm{ps}}$.

(b) Contribution proportional to n_f for $C_{a,q}^{\mathrm{ns}}$.

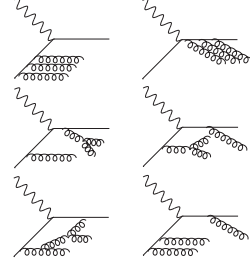Figure 20: $\mathcal{O}(\alpha_S^2)$ - $\gamma^* q_i \to q_i q_j \bar{q}_j$.

Figure 21: $\mathcal{O}(\alpha_S^3)$ - $\gamma^* q_i \to q_i ggg$. Contribution to $C_{a,q}^{\mathrm{ns}}$ not proportional to n_f.

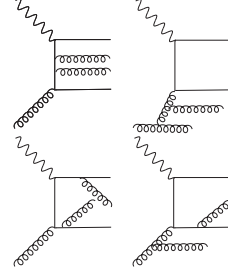Figure 22: $\mathcal{O}(\alpha_S^3)$ - $\gamma^* g \to q_j \bar{q}_j gg$.

where $a = \{2, L\}$, and

$$q_{\mathrm{ns}} = \sum_{i=1}^{n_f} (e_i^2 - \langle e^2 \rangle) q_i^+$$

$$q_{\mathrm{s}} = \sum_{i=1}^{n_f} q_i^+, \qquad q_i^+ = q_i + \bar{q}_i$$

$$\langle e^2 \rangle = \langle e^2 \rangle^{(n_f)} = \frac{1}{n_f} \sum_{i=1}^{n_f} e_i^2 \qquad , \qquad (\mathrm{B4})$$
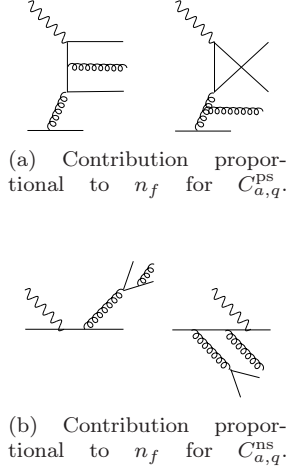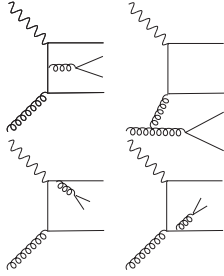
and $C_{a,q}^{\mathrm{ns}}$, $C_{a,q}^{\mathrm{s}}$, $C_{a,g}$ are the Wilson coefficients. From Eq. (B4) one can extract the contribution from a single initial-state quark as:

$$x^{-1} F_{a,q_i} = q_i^+ \otimes \left[e_i^2 \, C_{a,q}^{\mathrm{ns}} + \langle e^2 \rangle C_{a,q}^{\mathrm{ps}} \right] \qquad (\mathrm{B5})$$

where $C_{a,q}^{\mathrm{ps}}$ is

$$C_{a,q}^{\mathrm{ps}} = C_{a,q}^{\mathrm{s}} - C_{a,q}^{\mathrm{ns}} \qquad . \qquad (\mathrm{B6})$$

To further decompose Eq. (B5) into the different final-state contributions, we examine the diagrams that contribute to the non-singlet and purely-singlet coefficients. Diagrams in which the photon couples to the incoming quark contribute to $C_{a,q}^{\mathrm{ns}}$ (Figs. 15, 16, 18, 20b, etc.), whereas the diagrams where the photon does not couple to the incoming quark contribute to $C_{a,q}^{\mathrm{ps}}$; these contributions appear for the first time at $\mathcal{O}(\alpha_S^2)$ in Figs. 20a, 23a. Separating out the final-state quark from Eq. (B5) we

(a) Contribution proportional to n_f for $C_{a,q}^{\mathrm{ps}}$.

(b) Contribution proportional to n_f for $C_{a,q}^{\mathrm{ns}}$.

Figure 23: $\mathcal{O}(\alpha_S^3)$ - $\gamma^* q_i \to q_i q_j \bar{q}_j g$.

Figure 24: $\mathcal{O}(\alpha_S^3)$ - $\gamma^* g \to q_j \bar{q}_j q_k \bar{q}_k$.

obtain:

$$
x^{-1} F_a^{ij} = q_i^+ \otimes \bigg\{ e_i^2 \left[C_{a,q}^{\mathrm{ns}}(n_f = 0)\ \delta_{ij} \right.
$$
$$
\left. + C_{a,q}^{\mathrm{ns}}(j) - C_{a,q}^{\mathrm{ns}}(j-1) \right]
$$
$$
+ \langle e^2 \rangle^{(j)} C_{a,q}^{\mathrm{ps}}(j) - \langle e^2 \rangle^{(j-1)}\ C_{a,q}^{\mathrm{ps}}(j-1) \bigg\} . \tag{B7}
$$

We have introduced δ_{ij} in the non-singlet contribution to account for contributions in which the photon couples to the initial and final-state quark. When this is not the case, (i.e., in all purely-singlet contributions and in non-singlet contributions such as the ones in Fig. 20b), the difference of the coefficient functions with $n_f = j$ and $n_f = j - 1$ flavors is taken.

Some comments are in order:

- We have verified analytically and numerically that one recovers Eq. (B5) when summing over the final state quark partons ($j = 1, \ldots, n_f$) in Eq. (B7).

- The corresponding decomposition for the gluon-initiated subprocesses is simpler than the one in

Eq. (B7) since there are only purely-singlet contributions:

$$
x^{-1} F_a^{0j} = g \otimes \bigg\{ \langle e^2 \rangle^{(j)} C_{a,g}(j)
$$
$$
- \langle e^2 \rangle^{(j-1)}\ C_{a,g}(j-1) \bigg\} . \tag{B8}
$$

- We remark that the decomposition in Eq. (B7) also includes the contributions from virtual diagrams to the Wilson coefficients. As has been discussed in the literature [40], such a decomposition is ambiguous at $\mathcal{O}(\alpha_S^2)$ and beyond due to the treatment of heavy quark loops contributing to the light quark structure functions. However, numerically the ambiguous terms are small and it is standard to analyze the heavy quark structure functions $F_{2,L}^c$ and $F_{2,L}^b$ in addition to the inclusive structure functions $F_{2,L}$ without any further prescription.

For the general neutral current case (including Z-boson exchange), the electromagnetic couplings should be replaced by electroweak couplings as follows:

$$
e_i^2 \to a_{q_i}^+ = e_i^2 - 2 e_i v_e v_q \chi_Z + (v_e^2 + a_e^2)(v_q^2 + a_q^2)\chi_Z^2 \tag{B9}
$$

where

$$
v_f = T_f^3 - 2 Q_f\ \sin^2 \theta_W , \qquad a_f = T_3^f \tag{B10}
$$

are the standard (axial-)vector couplings of the Z-boson to the leptons ($f = e$) and quarks ($f = q$). Furthermore, χ_Z is the ratio of the Z-boson propagator with respect to the photon propagator including additional coupling factors:

$$
\chi_Z = \frac{G_F M_Z^2}{2\sqrt{2}\,\pi\,\alpha_{em}}\ \frac{Q^2}{Q^2 + M_Z^2}\quad . \tag{B11}
$$

Finally, the average squared charge is modified as

$$
\langle e^2 \rangle^{(n_f)} \to a^+(n_f) = \frac{1}{n_f} \sum_{i=1}^{n_f} a_{q_i}^+ \quad . \tag{B12}
$$

Appendix C: Matching Across Heavy Flavor Thresholds

As we compute at higher orders, we find the matching conditions of the PDFs become discontinuous at $\mathcal{O}(\alpha_s^2)$ (NNLO), and the matching of the $\overline{MS}$ $\alpha_s(\mu)$ becomes discontinuous at $\mathcal{O}(\alpha_s^3)$ (N³LO).

While the discontinuities in the PDFs and α_s (which are unphysical quantities) persist at all orders, physical observables (such as cross sections and structure functions) will match across thresholds up to the computed order of the perturbation theory; for example, a physical

observable in an N-flavor and an $(N + 1)$-flavor scheme will match up to higher order terms when computed to order α_s^M in the perturbation expansion:

$$\sigma^N = \sigma^{N+1} + \mathcal{O}(\alpha_s^{M+1}) \quad .$$

As it is not immediately obvious how the discontinuities cancel order-by-order, we shall examine a NNLO numeric case, and also a simple analytic example.

1. Discontinuities across the flavor transition.

To illustrate the behavior of the discontinuities, we will work at NNLO where the DGLAP evolution and the flavor-threshold boundary conditions have been computed and implemented.[14] Since $\mu = m_c$ is often used for the initial evolution scale, we will focus on the transition from $N_F = 4$ to $N_F = 5$ flavors at $\mu = m_b$.

The matching conditions across flavor thresholds can be summarized as [41]

$$f_a^{N+1} = A_{ab} \otimes f_b^N \tag{C1}$$

where f^N and f^{N+1} are the PDFs for N and $N + 1$ flavors, and A_{ab} can be expanded perturbatively. In the VFNS for $\mu < m_b$, the b-quark PDF is zero and the gluon PDF is finite and positive. Using Eq. (C1) for $\mu > m_b$, we find the b-quark is negative for $\mu \sim m_b$, and it becomes more negative as we move to smaller x. In contrast, the gluon has a positive discontinuity as it must to ensure the momentum sum rule is satisfied.

2. The b-quark flavor transition.

Although these discontinuities are too small to be noticeable in the figures of Sec.IV, in Figure 25 we have magnified the axes so the discontinuities are visible. Here, we display F_2 and F_L for a selection of x-values.

The first general feature we notice in Fig. 25 is that the size of the discontinuity generally grows as we go to smaller x values. This is consistent with the fact that the discontinuity computed by Eq. (C1) also grows for smaller x. We display the results for a selection of n-scaling values; note that the uncertainty arising from the discontinuity is typically on the order of the difference due to the choice of scaling.

Another feature that is most evident for the series of F_L plots (Fig. 25b) is that the discontinuity can change sign for different x values. This can happen because the mix of quark and gluon initiated terms is changing as a function of x.

This observation is key to understanding how the (unphysical) PDFs may have a relatively large discontinuity, while the effect on the physical quantities (such as σ and $F_{2,L}$) is moderated. Because physical quantities will contain a sum of gluon and quark initiated contributions, and because the discontinuity of the quark and gluon PDFs have *opposite signs*, the discontinuities of the quark and gluon PDFs can partially cancel so that the physical quantity may have a reduced discontinuity.

This discontinuity, in part, reflects the theoretical uncertainty of the perturbation theory at a given order. As we compute the physical observables to higher and higher orders, this discontinuity will be reduced even though the discontinuity in the PDFs and α_s remain. We will demonstrate this mechanism in the following.

3. A "Toy" Example at NLO"

We now illustrate how the cancellation of the quark and gluon PDF discontinuities work analytically using a "toy" calculation.

Expanding Eq. (C1) in the region of $\mu = m_b$ we have:

$$f_b^5 = \left\{ 0 + \frac{\alpha_s}{2\pi} P_{qg} (L + a_{qg}) + O(\alpha_s^2) \right\} \otimes f_g^4$$
$$f_g^5 = \left\{ 1 + \frac{\alpha_s}{2\pi} P_{gg} (L + a_{gg}) + O(\alpha_s^2) \right\} \otimes f_g^4$$
$$\tag{C2}$$

where $L = \ln(\mu^2/m_b^2)$. It happens that the constant terms a_{ij} in Eq. (C2) are zero at $\mathcal{O}(\alpha_s^1)$ in the $\overline{MS}$ scheme; this is not due to any underlying symmetry, and in fact at $\mathcal{O}(\alpha_s^2)$ these terms are non-zero. Because a_{ij} are zero, if we perform the matching at $\mu = m_b$, we find that the gluon PDF is continuous $f_b^5(x, m_b) = f_g^4(x, m_b)$, and the bottom PDF starts from zero $f_b^5(x, m_b) = 0$.

a. If a_{ij} was non-zero at $\mathcal{O}(\alpha_s^1)$

To illustrate how the discontinuities cancel in the ACOT renormalization scheme, we will suppose (for this "toy" calculation) that the constant terms (a_{ij}) in the matching conditions are non-vanishing at order α_s^1; thus, the gluon and bottom PDFs will now have $\mathcal{O}(\alpha_s^1)$ discontinuities, *but* the physical observables computed with different N_F values will still match up to $\mathcal{O}(\alpha_s^2)$.

In the ACOT scheme, the total cross section can be decomposed as: $\sigma_{TOT} = \sigma_{LO} + \sigma_{NLO} - \sigma_{SUB}$, where σ_{LO} represents $\gamma b \to b$, σ_{NLO} represents $\gamma g \to b\bar{b}$, and σ_{SUB} represents the $(g \to b) \otimes (\gamma b \to b)$ "subtraction" contribution.[15] We will now perturbatively compute σ_{TOT} in the region $\mu \sim m_b$ for both $N_F = 4$ and $N_F = 5$.

---

[14] At present, the full set of matching conditions and DGLAP kernels have not been computed at N^{3}LO.

[15] Note, we will focus on the gluon-initiated terms, but the demonstration for the quark-initiated pieces is analogous.
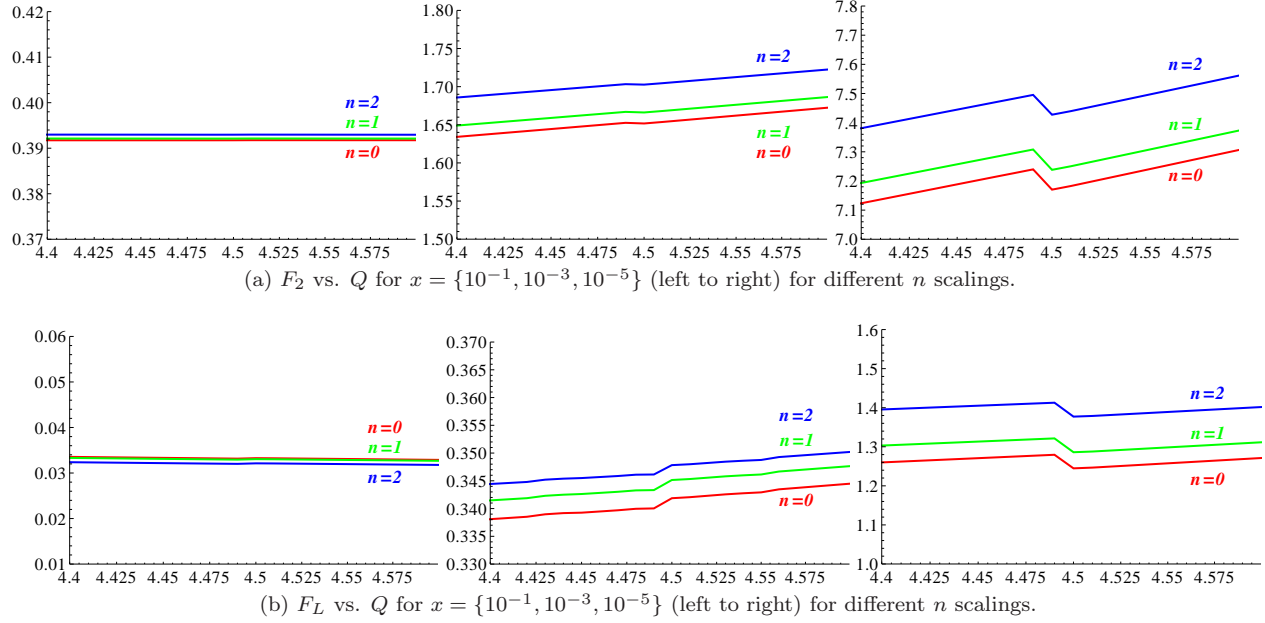
(a) F_2 vs. Q for $x = \{10^{-1}, 10^{-3}, 10^{-5}\}$ (left to right) for different n scalings.

(b) F_L vs. Q for $x = \{10^{-1}, 10^{-3}, 10^{-5}\}$ (left to right) for different n scalings.

Figure 25: Discontinuity for F_2, F_L at NNLO in the region of the bottom mass, $m_b = 4.5$ GeV.

b.   ACOT for $N_F = 4$

For $\mu < m_b$, we have $N_F = 4$ and $f_b = 0$; thus, σ_{LO} and σ_{SUB} vanish, and we have:

$$\sigma_{TOT}^{N_F=4} = \sigma_{NLO} = C^1 \otimes f_g^4 + O(\alpha_s^2)$$

where C^1 represents the $\mathcal{O}(\alpha_s^1)$ process $\gamma g \to b\bar{b}$.

c.   ACOT for $N_F = 5$

For $\mu > m_b$, we have $N_F = 5$ and $f_b \neq 0$. For the contributions we have:

$$\sigma_{LO} = C^0 \otimes f_b^5 \simeq C^0 \otimes \left\{ 0 + \frac{\alpha_s}{2\pi} P_{qg} (L + a_{qg}) \right\} \otimes f_g^4$$

$$\sigma_{NLO} = C^1 \otimes f_g^5 \simeq C^1 \otimes \left\{ 1 + \frac{\alpha_s}{2\pi} P_{gg} (L + a_{gg}) \right\} \otimes f_g^4$$

$$\sigma_{SUB} = C^0 \otimes \widetilde{f}_{g \to q} \otimes f_g^5 \simeq C^0 \otimes \left\{ \frac{\alpha_s}{2\pi} P_{qg} (L + a_{qg}) \right\}$$

$$\otimes \left\{ 1 + \frac{\alpha_s}{2\pi} P_{gg} (L + a_{gg}) \right\} \otimes f_g^4$$

Keeping terms to $\mathcal{O}(\alpha_s^1)$ we have:

$$\sigma_{TOT}^{N_F=5} = \sigma_{LO} + \sigma_{NLO} - \sigma_{SUB} = C^1 \otimes f_g^4 + O(\alpha_s^2)$$

Notice that the discontinuity introduced by a_{qg} in the PDFs is canceled by a_{qg} from the SUB contribution.[16]

---

[16] The explicit form of the ACOT subtraction is defined in Sec.IV.C (*cf.*, Eq. (36)) of Ref. [5]. For an example of the cancellation between σ_{LO} and σ_{SUB} in a more general context, see Ref. [42].

d.   Comparison of $N_F = 5$ and $N_F = 4$

Comparing the $N_F = 5$ and $N_F = 4$ results, we find

$$\sigma_{TOT}^{N_F=5} = \sigma_{TOT}^{N_F=4} + O(\alpha_s^2)$$

so that the total physical results match up the order of the perturbation theory.

In the above illustration, we have retained the log terms (L); the cancellation of the logs is ensured in a well defined renormalization scheme, and the a_{ij} constant terms get carried along with the logs and will thus cancel order by order.

Therefore, the discontinuity of the physical quantities $(\sigma, F_{2,L})$ reflects the perturbative uncertainty, and this will be systematically reduced at higher orders.

[1] I. Schienbein, V. A. Radescu, G. Zeller, M. Christy, C. Keppel, et al., J.Phys.G **G35**, 053101 (2008), 0709.1775.

[2] H1 and ZEUS Collaborations (2010), Reports Nos. H1prelim-10-044 and ZEUS-prel-10-008 (unpublished), http://www-h1.desy.de/psfiles/confpap/DIS2010/H1prelim-109044.pdf.

[3] F. D. Aaron et al., Eur. Phys. J. **C71**, 1579 (2011), 1012.4355.

[4] M. A. G. Aivazis, J. C. Collins, F. I. Olness, and W. K. Tung, Phys. Rev. **D50**, 3102 (1994), hep-ph/9312319.

[5] J. C. Collins, Phys. Rev. **D58**, 094002 (1998), hep-ph/9806259.

[6] S. Kretzer and I. Schienbein, Phys. Rev. **D58**, 094035 (1998), hep-ph/9805233.

[7] R. Thorne and R. Roberts, Phys.Lett. **B421**, 303 (1998), hep-ph/9711223.

[8] M. Krämer, F. I. Olness, and D. E. Soper, Phys. Rev. **D62**, 096007 (2000), hep-ph/0003035.

[9] R. M. Barnett, Phys. Rev. Lett. **36**, 1163 (1976).

[10] W. K. Tung, S. Kretzer, and C. Schmidt, J. Phys. **G28**, 983 (2002), hep-ph/0110247.

[11] S. Kretzer, H. Lai, F. Olness, and W. Tung, Phys.Rev. **D69**, 114005 (2004), hep-ph/0307022.

[12] M. Guzzi, P. M. Nadolsky, H.-L. Lai, and C.-P. Yuan (2011), 1108.5112.

[13] E. Laenen, S. Riemersma, J. Smith, and W. L. van Neerven, Nucl. Phys. **B392**, 162 (1993).

[14] M. Guzzi, P. M. Nadolsky, H.-L. Lai, and C. P. Yuan (2011), 1108.4008.

[15] R. Thorne and R. Roberts, Phys.Rev. **D57**, 6871 (1998), hep-ph/9709442.

[16] R. Thorne, Phys.Rev. **D73**, 054019 (2006), hep-ph/0601245.

[17] M. Cacciari, M. Greco, and P. Nason, JHEP **9805**, 007 (1998), hep-ph/9803400.

[18] S. Forte, E. Laenen, P. Nason, and J. Rojo, Nucl.Phys. **B834**, 116 (2010), 1001.2312.

[19] R. D. Ball, V. Bertone, F. Cerutti, L. Del Debbio, S. Forte, et al., Nucl.Phys. **B849**, 296 (2011), 1101.1300.

[20] J. Andersen et al. (SM and NLO Multileg Working Group), pp. 21–189 (2010), 1003.1241.

[21] T. Gottschalk, Phys. Rev. D **23**, 56 (1981).

[22] M. Gluck, S. Kretzer, and E. Reya, Phys.Lett. **B380**, 171 (1996), hep-ph/9603304.

[23] J. Blumlein, A. Hasselhuhn, P. Kovacikova, and S. Moch, Phys.Lett. **B700**, 294 (2011), 1104.3449.

[24] M. Buza and W. van Neerven, Nucl.Phys. **B500**, 301 (1997), hep-ph/9702242.

[25] W. Furmanski and R. Petronzio, Zeit. Phys. **C11**, 293 (1982).

[26] W. A. Bardeen, A. J. Buras, D. W. Duke, and T. Muta, Phys. Rev. **D18**, 3998 (1978).

[27] G. Altarelli, R. K. Ellis, and G. Martinelli, Nucl. Phys. **B143**, 521 (1978).

[28] W. L. van Neerven and E. B. Zijlstra, Phys. Lett. **B272**, 127 (1991).

[29] E. B. Zijlstra and W. L. van Neerven, Phys. Lett. **B273**, 476 (1991).

[30] E. B. Zijlstra and W. L. van Neerven, Nucl. Phys. **B383**, 525 (1992).

[31] J. A. M. Vermaseren, A. Vogt, and S. Moch, Nucl. Phys. **B724**, 3 (2005), hep-ph/0504242.

[32] W. L. van Neerven and A. Vogt, Nucl. Phys. **B568**, 263 (2000), hep-ph/9907472.

[33] W. L. van Neerven and A. Vogt, Nucl. Phys. **B588**, 345 (2000), hep-ph/0006154.

[34] S. Moch, J. A. M. Vermaseren, and A. Vogt, Nucl. Phys. **B646**, 181 (2002), hep-ph/0209100.

[35] J. Sanchez Guillen, J. Miramontes, M. Miramontes, G. Parente, and O. A. Sampayo, Nucl. Phys. **B353**, 337 (1991).

[36] S. Moch, J. A. M. Vermaseren, and A. Vogt, Phys. Lett. **B606**, 123 (2005), hep-ph/0411112.

[37] M. A. G. Aivazis, F. I. Olness, and W. K. Tung, Phys. Rev. **D50**, 3085 (1994), hep-ph/9312318.

[38] M. Botje, Comput. Phys. Commun. **182**, 490 (2011), 1005.1481.

[39] W. Giele, E. Glover, I. Hinchliffe, J. Huston, E. Laenen, et al., pp. 275–426 (2002), hep-ph/0204316.

[40] A. Chuvakin, J. Smith, and W. L. van Neerven, Phys. Rev. **D61**, 096004 (2000), hep-ph/9910250.

[41] M. Buza, Y. Matiounine, J. Smith, R. Migneron, and W. van Neerven, Nucl.Phys. **B472**, 611 (1996), hep-ph/9601302.

[42] F. I. Olness and R. J. Scalise, Phys.Rev. **D57**, 241 (1998), hep-ph/9707459.